

# Statistical Inconsistencies in the KiDS-450 Dataset

George Efstathiou and Pablo Lemos

*Kavli Institute for Cosmology Cambridge and Institute of Astronomy, Madingley Road, Cambridge, CB3 0HA.*

12 March 2022

## ABSTRACT

The Kilo-Degree Survey (KiDS) has been used in several recent papers to infer constraints on the amplitude of the matter power spectrum and matter density at low redshift. Some of these analyses have claimed tension with the *Planck*  $\Lambda$ CDM cosmology at the  $\sim 2 - 3\sigma$  level, perhaps indicative of new physics. However, *Planck* is consistent with other low redshift probes of the matter power spectrum such as redshift space distortions and the combined galaxy-mass and galaxy-galaxy power spectra. Here we perform consistency tests of the KiDS data, finding internal tensions for various cuts of the data at  $\sim 2.2 - 3.5\sigma$  significance. Until these internal tensions are understood, we argue that it is premature to claim evidence for new physics from KiDS. We review the consistency between KiDS and other weak lensing measurements of  $S_8$ , highlighting the importance of intrinsic alignments for precision cosmology.

## 1 INTRODUCTION

Precision observations of the cosmic microwave background radiation (CMB) by the Planck satellite (Planck Collaboration et al. 2014a, 2016a, hereafter P16) and other experiments (Hinshaw et al. 2013; Sievers et al. 2013; Story et al. 2013) have shown that the  $\Lambda$ CDM cosmology, with nearly scale invariant, adiabatic, Gaussian initial perturbations, provides an excellent description of our Universe. Measurements of weak lensing of the CMB (Planck Collaboration et al. 2016b) show further that the  $\Lambda$ CDM model remains a good description of the Universe down to a redshift of  $z \sim 2$ , where the CMB lensing kernel peaks.

It is, nevertheless, important to test the model at lower redshifts, particularly at redshifts  $z \lesssim 1$  when the Universe becomes dominated by dark energy. Deviations from the  $\Lambda$ CDM model at low redshift could potentially reveal evidence for dynamical dark energy or modifications to General Relativity (see Amendola et al. 2016, for a review).

Weak galaxy lensing is an important probe of the matter power spectrum at low redshifts (Blandford et al. 1991; Miralda-Escude 1991; Kaiser 1992). Several ambitious deep imaging projects have reported results recently. These include the Canada France-Hawaii Telescope Lensing Survey (CFHTLenS, Heymans et al. 2012, 2013; Joudaki et al. 2017), Deep Lens Survey (DLS, Jee et al. 2016), Dark Energy Survey (DES, Abbott et al. 2016; Troxel et al. 2017; DES Collaboration et al. 2017) and Kilo Degree Survey (KiDs, Hildebrandt et al. 2017; Köhlinger et al. 2017). Weak lensing analysis of these surveys can be used to constrain the parameter combination<sup>1</sup>  $S_8 = \sigma_8(\Omega_m/0.3)^{0.5}$ ,

which can be compared to the *Planck* value from P16<sup>2</sup>,  $S_8 = 0.825 \pm 0.016$  derived from the Planck temperature power spectrum, low multipole polarization and Planck lensing (TT+lowTEB+lensing, in the notation of P16). However, the weak galaxy lensing results span a range of values. The reanalysis of CFHTLenS by Joudaki et al. (2017) finds  $S_8 = 0.732^{+0.029}_{-0.031}$ ; Jee et al. (2016) find  $S_8 = 0.818^{+0.034}_{-0.026}$  from DLS; Abbott et al. (2016) find  $S_8 = 0.81 \pm 0.06$  from the DES Science Verification data; Hildebrandt et al. (2017) (hereafter H17) find  $S_8 = 0.745 \pm 0.039$  from a tomographic correlation function analysis of KiDs while Köhlinger et al. (2017) (hereafter K17) find  $S_8 = 0.651 \pm 0.058$  from a tomographic power spectrum analysis of KiDs. The DES Year 1 weak lensing analysis<sup>3</sup> (Troxel et al. 2017) gives  $S_8 = 0.789^{+0.024}_{-0.026}$ . Some of these values are in tension with *Planck*. For example, H17 find a  $2.3\sigma$  discrepancy between KiDs and *Planck*, while K17 find a  $3.2\sigma$  discrepancy. However, the results from these different surveys do not agree particularly well with each other (even when using the same shear catalogue), showing differences in the value of  $S_8$  at the  $\sim 2 - 2.5\sigma$  level.

A statistically significant tension between the *Planck*  $\Lambda$ CDM cosmology and weak galaxy lensing could have important consequences for fundamental physics (e.g. Joudaki et al. 2016). But how seriously should we take the weak lensing results? A minimal requirement is that a cosmic shear data set should be internally self-consistent. The main pur-

of the critical density  $\rho_c$  and  $h$  is the Hubble constant in units of  $100 \text{ km s}^{-1} \text{ Mpc}^{-1}$ .

<sup>2</sup> Unless stated otherwise, we quote  $\pm 1\sigma$  errors on parameters.

<sup>3</sup> DES Year 1 results (Troxel et al. 2017; DES Collaboration et al. 2017) appeared after the submission of this paper and so will not be discussed in detail.

<sup>1</sup> Where  $\sigma_8$  is the present day linear theory root-mean-square amplitude of the matter fluctuation spectrum averaged in spheres of radius  $8 h^{-1} \text{ Mpc}$ ,  $\Omega_m$  is the present day matter density in units

pose of this paper is to show that this does not seem to be the case with KiDS.

Before we begin, we make a few remarks concerning cosmic shear analysis. Most analyses involve estimation of correlation functions  $\xi_+$  and  $\xi_-$  as a function of relative angular separation  $\theta$ , or of the cosmic shear E-mode power spectrum  $P_\kappa(\ell)$  as a function of multipole  $\ell$ . These are related by

$$\xi_{\pm} = \frac{1}{2\pi} \int d\ell \ell P_\kappa(\ell) J_{0,4}(\ell\theta). \quad (1)$$

For a cross-power spectrum between redshift bins  $i$  and  $j$ , the shear power spectrum is related to the non-linear matter power spectrum  $P_\delta$  by

$$P_\kappa^{ij}(\ell) = \int_0^{\chi_H} d\chi \frac{q_i(\chi)q_j(\chi)}{[f_K(\chi)]^2} P_\delta \left( \frac{(\ell+1/2)}{f_K(\chi)}, \chi \right), \quad (2)$$

where (following the notation of H17)  $\chi$  is the comoving radial distance,  $f_K(\chi)$  is the comoving angular diameter distance to distance  $\chi$ , and  $q_i(\chi)$  is the lensing efficiency for tomographic redshift bin  $i$ :

$$q_i(\chi) = \frac{3H_0^2\Omega_m}{2c^2} \frac{f_K(\chi)}{a(\chi)} \int_\chi^{\chi_H} d\chi' n_i(\chi') \frac{f_K(\chi' - \chi)}{f_K(\chi')}, \quad (3)$$

where  $\chi_H$  is the comoving Hubble distance and  $n_i(\chi)$  is the effective (weighted) number density galaxies in redshift bin  $i$  normalized so that  $\int n_i(\chi) d\chi = 1$ . Even if the image analysis is assumed to be free of systematic errors and biases, inferences on cosmology require an accurate model of the redshift distribution  $n_i(\chi)$ , which in turn requires accurate calibration of the photometric redshifts used to define the redshift bin  $i$ . A key test of the accuracy of the photometric redshift calibrations would be to demonstrate consistency between distinct cross-correlations  $i, j$ . However, this is not straightforward because of intrinsic ellipticity alignments between neighbouring galaxies (II term) and between gravitation shear and intrinsic shear (GI term). The power spectra<sup>4</sup> of these terms are usually modelled as

$$P_{II}^{ij}(\ell) = \int_0^{\chi_H} d\chi F^2(z) \frac{n_i(\chi)n_j(\chi)}{[f_K(\chi)]^2} P_\delta \left( \frac{(\ell+1/2)}{f_K(\chi)}, \chi \right), \quad (4a)$$

$$P_{GI}^{ij}(\ell) = \int_0^{\chi_H} d\chi F(z) \frac{(q_i(\chi)n_j(\chi) + n_i(\chi)q_j(\chi))}{[f_K(\chi)]^2} \times P_\delta \left( \frac{(\ell+1/2)}{f_K(\chi)}, \chi \right), \quad (4b)$$

(Hirata & Seljak 2004; Bridle & King 2007). In these equations,

$$F(z) = -A_{IA} C \rho_c \frac{\Omega_m}{D(z)}, \quad (4c)$$

where  $D(z)$  is the linear growth rate of perturbations normalized to unity at the present day, and  $C$  is a normalizing constant, usually chosen to be  $C = 5 \times 10^{-14} h^{-2} M_\odot^{-1} \text{Mpc}^3$ . With this choice, the intrinsic alignment amplitude is expected to be of order unity (and positive if intrinsic ellipticities are aligned with the stretching axis of the tidal field). This model of intrinsic alignments is heuristic and

<sup>4</sup> Neglecting B-modes.

simplified (see Blazek et al. (2017) for a more complex alignment model). Even in the context of this model, the intrinsic alignment amplitude may vary with redshift, luminosity, and galaxy type. For current weak lensing surveys, intrinsic alignments are not benign. The contributions of eqs. 4a and 4b are comparable to any claimed tensions between the *Planck* value of  $S_8$  and those inferred from cosmic shear surveys (with positive  $A_{IA}$  tending to raise the value of  $S_8$  and negative values lowering  $S_8$ ). How can we test the intrinsic alignment model? The conventional solution is to introduce additional nuisance parameters to characterize uncertainties in the intrinsic alignment model (e.g. Kirk et al. 2012), relying on the redshift dependence of the measured signals to disentangle true cosmic shear from intrinsic alignments. This, of course, requires accurate knowledge of the redshift distributions and their errors.

Current cosmic shear data is still relatively sparse, with a small number of measurements in coarse redshift bins. The number of internal consistency checks of the data and the various components of the model (including nuisance parameters) is therefore limited<sup>5</sup>. In Section 2, we perform consistency tests of the KiDS data from H17. In Section 3 we compare the KiDS results with *Planck* and measurements of redshift space distortions and rich cluster abundances, which provide independent measures of the amplitude of the matter fluctuations at similar redshifts to those of the KiDS galaxies. Section 4 compares the results from various weak lensing analyses. Our main conclusions are presented in Section 5.

## 2 TESTS OF THE KIDS DATA

We use the KiDS cross-correlation measurements of  $\xi_+$  and  $\xi_-$  in four tomographic redshift bins as reported by H17 together with the associated CosmoMC likelihood module and covariance matrix<sup>6</sup>. For reference, the four redshift bins span the following ranges in photometric redshift  $z_B$ :  $0.1 < z_B \leq 0.3$  (bin 1),  $0.3 < z_B \leq 0.5$  (bin 2),  $0.5 < z_B \leq 0.7$  (bin 3),  $0.7 < z_B \leq 0.9$  (bin 4). We used the same angular ranges, photometric redshift calibrations and errors, nuisance parameters and priors as in ‘fiducial’ analysis in H17 (first entry in their Table 4) and verified that we recovered the identical best-fit  $\chi^2$  (162.8) and constraint on  $S_8$  ( $S_8 = 0.745 \pm 0.039$ ). We then removed all cross-correlations involving one of the photometric redshift bins. The results are summarized in Table 1 and in Fig. 1.

The first point to note is that the intrinsic alignment amplitude is reasonably stable to the removal of photometric redshift bins. All of the posteriors shown in Fig. 1 are consistent with the intrinsic alignment solution from the full dataset ( $A_{IA} = 1.10^{+0.68}_{-0.54}$ ). However, it is also clear that redshift bin 4 carries a high weight in fixing  $A_{IA}$ . With redshift bin 4 removed, the posterior distribution develops a long tail to negative values that is cut-off by the lower end of the  $A_{IA}$

<sup>5</sup> The situation is very different to the CMB, where there is a large amount of information to separate a high amplitude frequency independent cosmological signal with a distinctive power spectrum from low amplitude foregrounds with smooth power spectra.

<sup>6</sup> Downloaded from <http://kids.strw.leidenuniv.nl>.

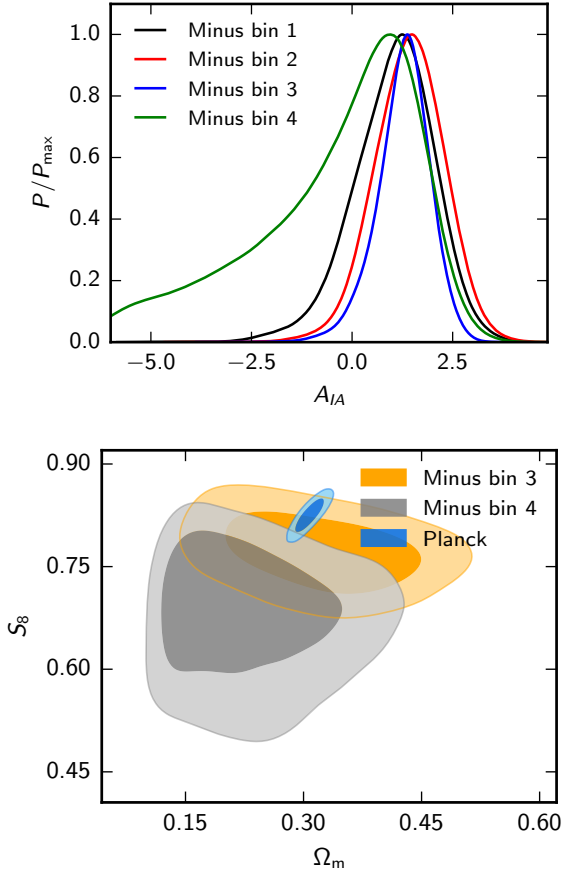


**Figure 1.** The upper panel shows the posteriors for the intrinsic alignment parameter  $A_{IA}$  (equ. 4c) as we remove all cross-correlations involving a particular redshift bin. The lower panel shows the 68 and 95% constraints on  $S_8$  for the data minus redshift bin 3 (orange) and minus redshift bin 4 (grey). The blue contours show the *Planck* constraints from the TT+lowTEB+lensing data combination as given in P16.

**Table 1.** Conditional  $\chi^2$  tests removing photometric redshift bins

$\mathbf{y}^D$	$S_8$	$A_{IA}$	$\chi^2_{\text{cond}}$	$N_{\sigma_{\text{cond}}}$
minus z-bin 1	$0.745 \pm 0.040$	$1.14 \pm 0.85$	61.0 (52)	0.89
minus z-bin 2	$0.754 \pm 0.042$	$1.24 \pm 0.80$	66.3 (52)	1.40
minus z-bin 3	$0.771 \pm 0.039$	$1.25 \pm 0.57$	78.2 (52)	2.60
minus z-bin 4	$0.684 \pm 0.071$	$-0.1 \pm 1.7$	87.9 (52)	3.52
minus $\xi_-$	$0.778 \pm 0.040$	$1.10 \pm 0.73$	89.7 (60)	2.71
minus $\xi_+$	$0.705 \pm 0.048$	$0.92 \pm 0.97$	84.1 (70)	1.20

Notes: The first column defines the portion of the data vector ( $\mathbf{y}^D$ ) used to fit the model. The second and third columns give the marginalised mean values of  $S_8$ ,  $A_{IA}$  and their  $1\sigma$  errors. The fourth column gives the conditional  $\chi^2_{\text{cond}}$ , as defined in equ. 11, for the rest of data vector,  $\mathbf{x}^D$ . The numbers in parentheses list the length,  $N_x$ , of the vector  $\mathbf{x}^D$ . The fifth column gives the number of standard deviations by which  $\chi^2_{\text{cond}}$  differs from  $N_x$ ,  $N_{\sigma_{\text{cond}}} = (\chi^2_{\text{cond}} - N_x)/\sqrt{2N_x}$ .

prior (uniform between  $-6 < A_{IA} < 6$ ). As a consequence of this long tail, the best fit value of  $S_8$  with bin 4 removed is driven to lower values and its error increases substantially compared to the full sample (lower panel of Fig. 1 and Table 1). Redshift bin 4 is therefore critical in pinning down the intrinsic alignment solution and reducing the error on  $S_8$ .

If redshift bin 3 is removed,  $S_8$  rises and the constraints in the  $S_8 - \Omega_m$  plane become compatible with *Planck* (Fig. 1). This is not unexpected, because one can see from Fig. 5 of H17 that the best-fit fiducial model tends to sit high for all cross-spectra involving tomographic redshift bin 3 (particularly for  $\xi_-$ ). With redshift bin 3 removed, there is substantial overlap in the posteriors in the  $S_8 - \Omega_m$  plane with those from the full sample and with the other subsets of the data summarized in Table 1. However, these various estimates of  $S_8$  are highly correlated since they share common data. Are the parameter shifts seen in these subsets statistically reasonable? We turn to this question next.

We can perform a more elaborate statistical consistency test by dividing the data vector into two components:

$$\mathbf{z}^D = (\mathbf{x}^D, \mathbf{y}^D). \quad (5)$$

We can then fit  $\mathbf{y}^D$  to a model (including nuisance parameters),  $\hat{\mathbf{y}}$ . The model parameters also make a theory prediction for the data partition  $\mathbf{x}^D$ , which we denote  $\hat{\mathbf{x}}$ . We can then write the theory vector for  $\mathbf{z}^D$  as

$$\hat{\mathbf{z}} = (\lambda \hat{\mathbf{x}}, \hat{\mathbf{y}}), \quad (6)$$

introducing a new parameter  $\lambda$ . Evidently, if the data partitions and model are consistent, the new parameter  $\lambda$  should be consistent with unity. The tests described in this Section are all based on the  $\Lambda$ CDM model, *but with a free amplitude*. Since cosmic shear measurements have very limited ability to fix shape parameters, and the data cuts that we apply cover similar redshift ranges, it seems reasonable to interpret differences in  $\lambda$  as indicative of systematic errors in the data. To recap, we run MCMC chains to determine the model parameters from a data partition  $\mathbf{y}^D$  and determine a single amplitude parameter  $\lambda$  by fitting to the rest of the data  $\mathbf{x}^D$ . The posterior distributions of  $\lambda$  for the data cuts of Table 1 are shown in Fig. 2.

The upper plot in Fig. 2 compares the amplitudes  $\lambda_-$  (fitting the model parameters to  $\xi_+$ ) and  $\lambda_+$  (fitting the model parameters to  $\xi_-$ ). This agrees with the visual impression given by Fig. 5 of H17, namely that  $\xi_-$  wants a low amplitude while  $\xi_+$  prefers a high amplitude. Integrating these distributions,

$$\int_0^1 P(\lambda_-) d\lambda_- = 2.9 \times 10^{-3}, \quad (7a)$$

$$\int_1^\infty P(\lambda_+) d\lambda_+ = 4.2 \times 10^{-2}. \quad (7b)$$

A value of  $\lambda = 1$  therefore lies in the tails of both posterior distributions. These results show that  $\xi_-$  sits about  $2.8\sigma$  low compared to the best fit  $\Lambda$ CDM cosmology determined from  $\xi_+$ .

The lower plot in Fig. 2 tests consistency between photometric redshift bins including both  $\xi_+$  and  $\xi_-$  in the fits. The parameters  $\lambda_i$  (with  $i$  running from 1 – 4) are computed for data partitions in which  $\mathbf{y}^D$  excludes all cross-correlations involving photometric redshift bin  $i$ . In this test,

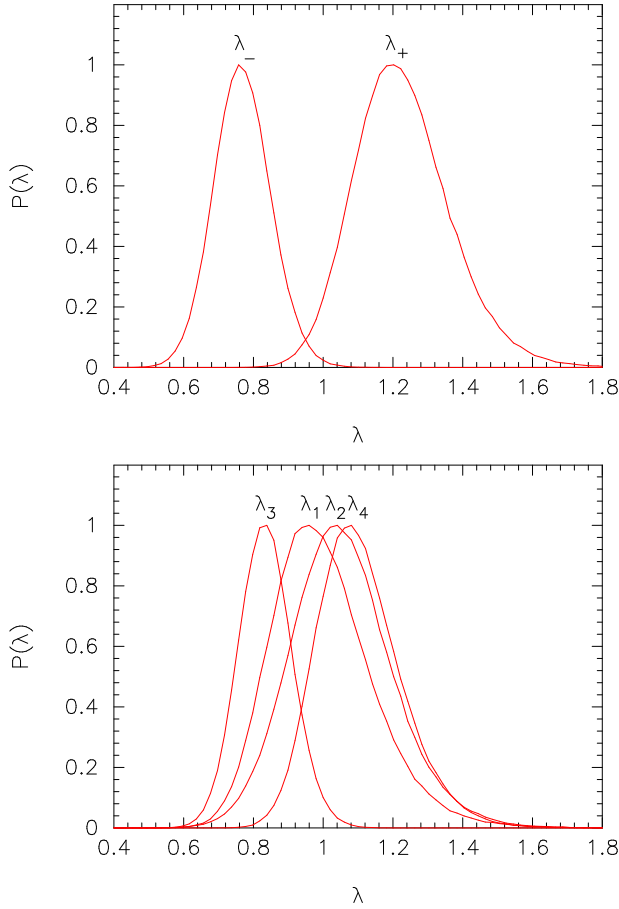


**Figure 2.** Posterior distributions of the parameter  $\lambda$  defined in Equ. 6. The upper figure shows the distributions if the model parameters are fitted to  $\xi_+$  (denoted  $\lambda_-$ ) and to  $\xi_-$  (denoted  $\lambda_+$ ). The lower figure shows the posterior distributions of  $\lambda$  for partitions of the data in which all cross-correlations involving a particular tomographic redshift bin are removed from the fit to the theoretical model (e.g.  $\lambda_3$ , corresponds to a theoretical model fitted to all cross-correlations that do not involve tomographic redshift bin 3).

photometric redshift bin 3 is an outlier with

$$\int_0^1 P(\lambda_3) d\lambda_3 = 1.3 \times 10^{-2}, \quad (7c)$$

suggesting that the data involving photometric redshift bin 3 is inconsistent with the rest of the data at about the  $2.2\sigma$  level. Again, this accords with the visual impression from Fig. 5 of H17, which shows that cross-correlations in both  $\xi_+$  and  $\xi_-$  involving photometric redshift bin 3 tend to lie below their best fit model.

Instead of using an amplitude parameter  $\lambda$ , we can and make a prediction for the vector  $\mathbf{x}^D$  conditional on the fit to  $\mathbf{y}^D$

$$\mathbf{x}^{\text{cond}} = \hat{\mathbf{x}} + \mathbf{C}_{xy} \mathbf{C}_{yy}^{-1} (\mathbf{y}^D - \hat{\mathbf{y}}). \quad (8)$$

If the best-fit model is known exactly, the covariance of  $\mathbf{x}^{\text{cond}}$  is

$$\mathbf{C}_{xx}^{\text{cond}} = \mathbf{C}_{xx} - \mathbf{C}_{xy} \mathbf{C}_{yy}^{-1} \mathbf{C}_{yx}. \quad (9)$$

However, in our application the best-fit model is determined

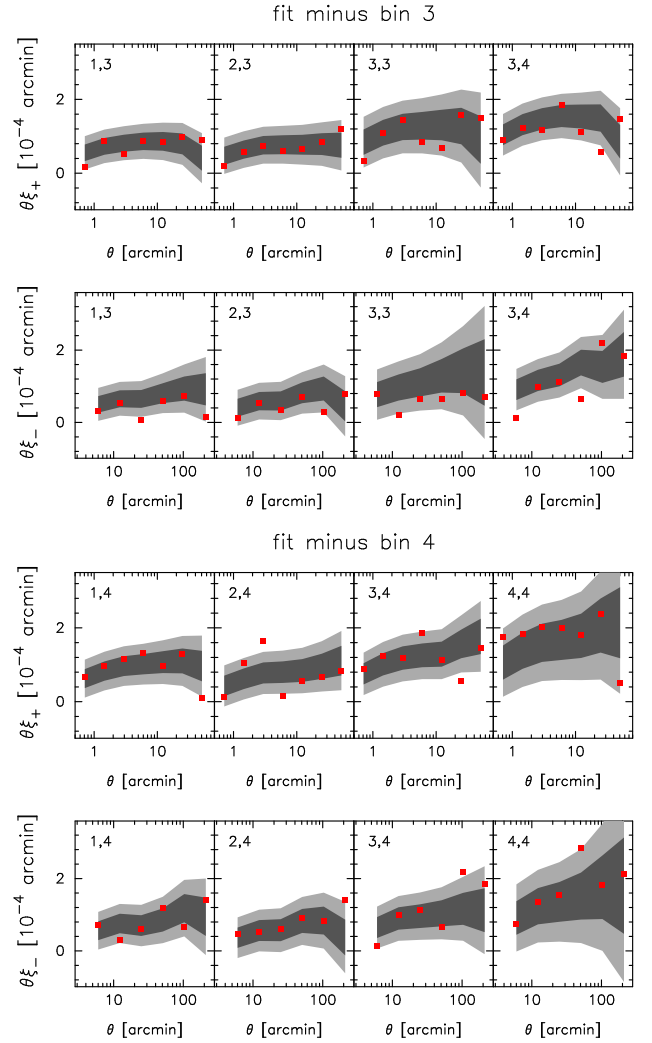


**Figure 3.** The upper two panels show cross-correlations  $\xi_+$  and  $\xi_-$  involving tomographic redshift bin 3 (red points). The numbers in each plot identify the cross-correlation (e.g. 1,3 denotes redshift bin 1 crossed with redshift bin 3). The grey bands show the allowed  $\pm 1\sigma$  (dark grey) and  $\pm 2\sigma$  (light grey) ranges allowed by the fits to the rest of the data. The lower two panels show the equivalent plots, but for cross-correlations involving tomographic redshift bin 4.

by fitting the data vector  $\mathbf{y}^D$  and so the uncertainty in the best-fit model contributes an additional variance to  $\mathbf{C}_{xx}^{\text{cond}}$ :

$$\mathbf{C}'_{xx}{}^{\text{cond}} = \mathbf{C}_{xx}^{\text{cond}} + \Delta \mathbf{C}_{xx}^{\text{cond}}, \quad (10)$$

which we determine empirically by sampling over the MCMC chains. In our application,  $\Delta \mathbf{C}_{xx}^{\text{cond}}$  is a small correction to  $\mathbf{C}_{xx}^{\text{cond}}$ .

As a test of the consistency of the data we compute a conditional  $\chi^2$ :

$$\chi_{\text{cond}}^2 = (\mathbf{x}^D - \mathbf{x}^{\text{cond}})^T (\mathbf{C}'_{xx}{}^{\text{cond}})^{-1} (\mathbf{x}^D - \mathbf{x}^{\text{cond}}). \quad (11)$$

The results of these tests are summarized in Table 1 and are consistent with the  $\lambda$ -tests shown in Fig. 2. Eliminating  $\xi_-$  leads to a substantial increase in  $S_8$  that is incompatible with  $\xi_-$  at about  $2.7\sigma$ . The redshift bin 3 component of the data vector is inconsistent with the rest of the data vector at about  $2.6\sigma$ . However, the  $\chi_{\text{cond}}^2$  reveals a new inconsis-



tency: the redshift bin 4 component of the data vector is inconsistent with the rest of the data vector at about  $3.5\sigma$ .

The origin of the high values of  $\chi^2_{\text{cond}}$  for these various partitions of the data vector is clear from Fig. 3. The figure shows the data vector (red points) for all cross-correlations involving redshift bin 3 (upper two panels) and those involving redshift bin 4 (lower two panels) compared to the expectations  $\mathbf{x}^{\text{cond}}$  conditional on the rest of the data (equ. 8). The grey bands show  $\pm 1$  and  $\pm 2\sigma$  ranges around  $\mathbf{x}^{\text{cond}}$  computed from the diagonal components of equ. 10. The top two panels of Fig. 3 show that cross-correlations involving redshift bin 3 want a lower amplitude than the rest of the data. This problem is particularly acute for  $\xi_-$  for the (3,3) and (3,4) redshift bin cross-correlations. These two cross-correlations carry quite high weight in fits to the full data vector (driving  $S_8$  down), yet they are inconsistent at nearly  $\sim 2.6\sigma$  with the rest of the data. A possible explanation for this discrepancy is an inaccuracy in the calibration of the photometric redshifts for bin 3. In fact van Uitert et al. (2017) present evidence for a  $2.3\sigma$  negative shift of  $\Delta z \approx -0.06$  for this redshift bin. They find no evidence for significant shifts in the other redshift bins.

As summarized in Table 1, removing redshift bin 4 lowers the value of  $S_8$  but increases the errors on  $S_8$  substantially because the intrinsic alignment amplitude is less well constrained. From Fig. 3 this low amplitude solution appears to match reasonably well with the general shape of the rest of the data vector, but now we see a high value of  $\chi^2_{\text{cond}}$  arising from outliers. In the lower two panels of this figure, 8 out of 52 data points sit outside the conditional  $\pm 2\sigma$  range<sup>7</sup>. Several of these outliers are at large angular scales and are not obvious in plots using errors computed from the diagonals of the full covariance matrix (e.g. Fig. 5 of H17). However, the KiDS covariance matrix tells us that the data vector should be correlated across different tomographic redshift bins. What Fig. 3 shows is that the KiDS correlation functions display significantly higher variance than expected from the KiDS covariance matrix, particularly at large angular scales and for correlations involving redshift bin 4. This excess variance is a serious problem because it means that the KiDS errors on cosmological parameters are systematically underestimated, especially if data at small angular scales is excluded.

Our analysis shows strong evidence for a statistical inconsistency between the KiDS estimates of  $\xi_+$  and  $\xi_-$ . H17 and van Uitert et al. (2017) find evidence for non-zero B-modes in the KiDS data at small angular scales ( $\theta < 4.2'$ ), indicative of systematics. If systematic errors contribute equally to the tangential and cross distortions (and this has not been demonstrated for KiDS), then the B-modes will affect  $\xi_+$ , but not  $\xi_-$ . Eliminating  $\xi_+$  entirely from the fits lowers  $S_8$  to  $0.705 \pm 0.048$  (see Table 1) with  $\chi^2 = 82.2$  for 50 degrees of freedom (a  $3.2\sigma$  excess). In other words, if one argues that the difference between  $\xi_+$  and  $\xi_-$  is indicative of systematic errors in  $\xi_+$ , then the tension between KiDS and *Planck* is exacerbated.

<sup>7</sup> Assuming Gaussian statistics, the  $p$ -value for this is about  $2.4 \times 10^{-3}$ .

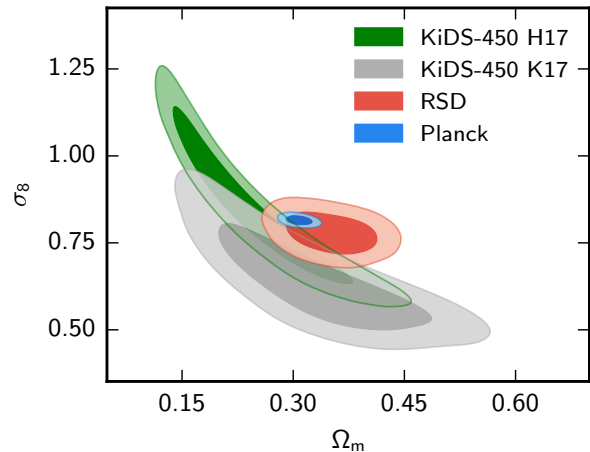


**Figure 4.** Constraints in the  $\sigma_8 - \Omega_m$  plane assuming the spatially flat  $\Lambda$ CDM cosmology. The 68% and 95% contours from *Planck* are shown in blue. The constraints from the H17 fiducial KiDS analysis are shown in green. The grey contours show the constraints from the power-spectrum analysis of KiDS reported by K17. The red contours show the constraints from redshift-space distortions (RSD) as discussed in the text.

### 3 COMPARISON WITH OTHER TECHNIQUES FOR MEASURING THE AMPLITUDE OF THE FLUCTUATION SPECTRUM

The results of the previous section show that there are some worrying internal inconsistencies in the KiDS dataset as analysed in H17. These inconsistencies suggest that we should be cautious in interpreting the KiDS constraints on cosmology. However, the tests in themselves do not tell us the causes of the inconsistencies, or their impact on the estimates of  $S_8$ . Is the amplitude of the matter fluctuations at redshifts  $z \lesssim 1$  really lower than expected in the *Planck*  $\Lambda$ CDM cosmology?

Another way of studying the amplitude of the matter power spectrum is via redshift space distortions (RSD, Kaiser 1987). RSD provide a measurement of the parameter combination  $f\sigma_8$ , where  $f$  is the logarithmic derivative of the linear growth rate with respect to the scale factor

$$f = \frac{d \ln D}{d \ln a}, \quad (12)$$

and  $a = (1+z)^{-1}$ . In the  $\Lambda$ CDM model,  $f \approx \Omega_m(z)^{0.55}$  and so RSD measure the parameter combination  $\sigma_8 \Omega_m^{0.55}$ , *i.e.* similar to the parameter combination  $S_8$  up to a known constant. Measurements of RSD from the DR12 analysis of the Baryon Oscillation Spectroscopy Survey (BOSS) have been reported by Alam et al. (2016). These measurements are for three redshift slices with effective redshifts  $z_{\text{eff}} = 0.38$ ,  $z_{\text{eff}} = 0.51$  and  $z_{\text{eff}} = 0.61$ , substantially overlapping with the redshift range of the KiDS survey. Huterer et al. (2017) have recently used the Supercal Type Ia supernova compilation (Scolnic et al. 2015) together with independent distance measurements of galaxies (Springob et al. 2014) to measure  $f\sigma_8$  at  $z_{\text{eff}} = 0.02$ . The *Planck*  $\Lambda$ CDM cosmology is in excellent agreement with these measurements of  $f\sigma_8$  over the entire redshift range  $z = 0.02 - 0.61$ . The consistency

between *Planck* and the RSD measurements is illustrated in Fig. 4, where we have combined the BOSS and Supercal RSD measurements to produce constraints in the  $\sigma_8 - \Omega_m$  plane<sup>8</sup>. The RSD constraints are in mild tension with the KiDS correlation function analysis of H17, and in even greater tension with the tomographic power-spectrum analysis of KiDS described by K17 *using the same shear catalogue*.

The abundance of rich clusters of galaxies (selected at various wavelengths) has been used in a number of studies to constrain the amplitude of the fluctuations spectrum at low redshift (e.g. Vikhlinin et al. 2009; Rozo et al. 2010; Hasselfield et al. 2013; Planck Collaboration et al. 2014b; Mantz et al. 2015; Planck Collaboration et al. 2016c; de Haan et al. 2016). As summarized in several of these papers, calibration of cluster masses is a major source of uncertainty in this type of analysis. Two recent studies (Mantz et al. 2015; de Haan et al. 2016) use weak gravitational lensing mass estimates from the ‘Weighing the Giants’ programme (von der Linden et al. 2014; Kelly et al. 2014; Applegate et al. 2014) to calibrate cluster scaling relations. Mantz et al. (2015) use an X-ray selected sample of clusters from the ROSAT All-Sky Survey covering the redshift range  $0 < z < 0.5$ , finding  $\sigma_8(\Omega_m/0.3)^{0.17} = 0.81 \pm 0.03$ . de Haan et al. (2016) use a sample of clusters identified with the South Pole Telescope with median redshift  $z_{\text{med}} = 0.53$  to infer  $\sigma_8(\Omega_m/0.27)^{0.3} = 0.797 \pm 0.031$ . Both of these estimates are consistent with the Planck P16  $\Lambda$ CDM cosmology:  $\sigma_8(\Omega_m/0.3)^{0.17} = 0.818 \pm 0.009$ ,  $\sigma_8(\Omega_m/0.27)^{0.3} = 0.848 \pm 0.012$ . Thus, there is no convincing evidence for any discrepancy between rich cluster counts and the expectations from the *Planck*- $\Lambda$ CDM cosmology. The de Haan et al. (2016) study is particularly interesting because it covers a similar redshift range to those of the BOSS RSD and KiDS measurements, yet is consistent with *Planck* and RSD.

#### 4 COMPARISON OF WEAK LENSING ESTIMATES OF $S_8$ : THE IMPORTANCE OF INTRINSIC ALIGNMENTS

Fig. 4 shows a discrepancy between the H17 and K17 analyses, which are based on the same shear catalogue. There is little doubt that the H17 and K17 analyses are incompatible, since not one of the 14,469 samples in the K17 MCMC likelihood chain<sup>9</sup> has parameters close to those of the best fit found by H17. In fact, van Uitert et al. (2017) (hereafter vU17) have computed cross power-spectra from  $\xi_+$  and  $\xi_-$  for the KiDS data using the identical redshift bins to those used in K17. Their auto-spectrum for the highest redshift bin differs substantially from the quadratic estimate of K17. The origin of this difference is not understood<sup>10</sup>. Another

pointer that the K17 results are affected by systematic errors comes from the intrinsic alignment solution. K17 find  $A_{IA} = -1.72^{+1.49}_{-1.25}$  which has the opposite (and from the theoretical perspective, counterintuitive) sign to that found by H17. This difference drives down the amplitude of  $S_8$  in the K17 analysis. Both the direct comparison of spectra reported by van Uitert et al. (2017) and the shift to a negative intrinsic alignment amplitude suggest that the K17 analysis is suspect.

The key point that we want to emphasise here is that the intrinsic alignment parameter  $A_{IA}$  is not a benign ‘nuisance’ parameter (for reviews see e.g. Troxel & Ishak 2015; Joachimi et al. 2015). The modelling of intrinsic alignments is degenerate with the cosmological parameters of interest,  $\sigma_8$ ,  $\Omega_m$ , and  $S_8$ , and so the model and associated parameters matter. Systematic errors in the data can be absorbed by the intrinsic alignment model and this will have an impact on cosmology. For example, van Uitert et al. (2017) have noted that the parameter  $A_{IA}$  can absorb systematic errors in the calibrations of photometric redshift distributions. (This can also be inferred from Fig. 1 which shows the sensitivity of the intrinsic alignment solution for the KiDS data to the highest photometric redshift bin). Implausible (e.g. strongly negative) values of  $A_{IA}$  suggest systematic errors and should therefore be followed up.

As an example, one of the lowest weak lensing determinations of  $S_8$  comes from the reanalysis of the revised CFHTLenS data (Joudaki et al. 2016). However, these authors find a strongly negative value of  $A_{IA} = -3.6 \pm 1.6$ , a value which seems unlikely for any reasonable mix of galaxy types. The recent DES analysis of Troxel et al. (2017) uses a redshift dependent amplitude:  $A_{IA}[(1+z)/(1.62)]^\eta$ , finding  $A_{IA} = 1.3^{+0.5}_{-0.6}$ ,  $\eta = 3.7^{+1.0}_{-2.3}$ <sup>13</sup>. Troxel et al. (2017) also test a more elaborate ‘mixed’ alignment model based on the work of Blazek et al. (2017). This model leads to a downward shift of  $S_8$  by about  $1\sigma$ , demonstrating that uncertainties in the modelling of intrinsic alignments makes a non-negligible contribution to the errors in cosmological parameters.

Returning to the KiDS survey, one way of achieving better control of intrinsic alignments and photometric redshift calibration errors is to add additional types of data. vU17 have analysed the shear power spectra from KiDS,  $P^E$  (constructed by integrating over  $\xi_+$  and  $\xi_-$ ). In addition, they use the Galaxies Mass Assembly (GAMA) redshift survey (Driver et al. 2011; Liske et al. 2015) to compute the galaxy-mass power-spectra,  $P^{gm}$  by cross-correlating the

(which are known to be present in the KiDS data). Inaccurate noise estimation would primarily affect the auto-spectra, where the noise levels are high compared to the cosmological signal (see Fig. 4 of H17).

<sup>12</sup> Note that the Jee et al. (2016) ‘baseline’ analysis of DLS use a luminosity dependent model of intrinsic alignments and impose a flat prior of  $5.14 < A_{IA} < 6.36$ , motivated by the results of Joachimi et al. (2011). However, they find that their results on  $S_8$  are insensitive to  $A_{IA}$  (see their Fig. 12), presumably because of the huge depth of DLS.

<sup>13</sup> These constraints become  $A_{IA} = 0.5^{+0.32}_{-0.38}$ ,  $\eta = 0^{+2.7}_{-2.8}$  with the addition of galaxy-galaxy and galaxy-shear data, DES Collaboration et al. (2017). These authors argue that an amplitude of  $A_{IA} \sim 0.5$  is consistent with their selection criteria if only red galaxies contribute to the intrinsic alignments.

<sup>8</sup> This is done using the final\_consensus\_dV\_FAP\_fsig data files and covariance matrix downloaded from [https://sdss3.org/science/booss\\_publications.php](https://sdss3.org/science/booss_publications.php). We then scanned the likelihood, using uniform priors in  $H_0$  and  $\Omega_m h^2$  to rescale the BOSS distance  $D_V$  and Alcock-Paczynski (Alcock & Paczynski 1979) parameter  $F_{AP}$  to the fiducial sound horizon used in the BOSS analysis, fixing  $\Omega_b h^2$  to the P16  $\Lambda$ CDM value.

<sup>9</sup> KiDS450\_QE\_EB\_4bins\_3zbins\_basez\_ia\_bary\_nu.txt, downloaded from <http://kids.strw.leidenuniv.nl>.

<sup>10</sup> Note that the quadratic estimator used by K17 is sensitive to noise estimation, particularly if there are B-mode systematics

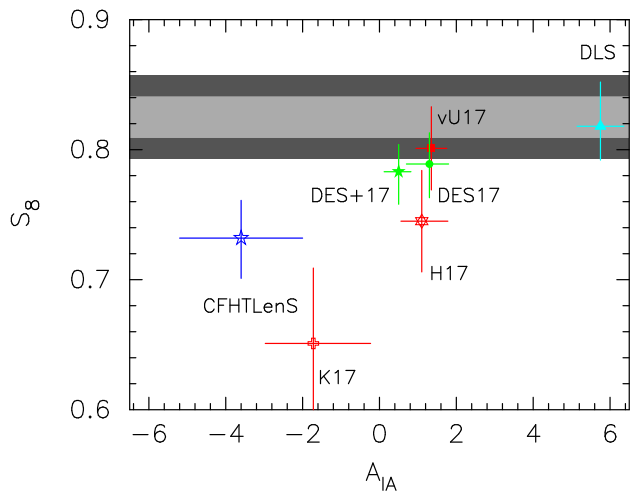


**Figure 5.**  $S_8$  plotted against the intrinsic alignment amplitude for various surveys together with  $1\sigma$  errors on  $S_8$  and  $A_{IA}$ . The grey bands show the  $1\sigma$  and  $2\sigma$  constraints from *Planck*. The data points are as follows: CFHTLenS (Joudaki et al. 2017); DLS (Jee et al. 2016)<sup>12</sup>; K17 shows the power spectrum analysis of KiDS (Köhlinger et al. 2017); H17 shows the correlation function analysis of KiDS (Hildebrandt et al. 2017); vU17 shows the constraints from combining  $P^{gg}$ ,  $P^{gm}$  and  $P^E$  measurements from KiDS and GAMA data (van Uitert et al. 2017); DES17 shows the cosmic shear constraints from DES year 1 data (Troxel et al. 2017) (note that the DES analyses uses a redshift dependent model of intrinsic alignments, as described in the text); DES+17 shows the combination of DES year 1 cosmic shear results with galaxy-galaxy and galaxy-shear measurements (DES Collaboration et al. 2017).

KiDS shear measurements with GAMA galaxies, and the galaxy-galaxy power spectra  $P^{gg}$ . From  $P^{gm} + P^{gg}$ , they find  $S_8 = 0.853 \pm 0.042$ . Combining with  $P^E$ , they find  $A_{IA} = 1.30 \pm 0.40$  and  $S_8 = 0.801 \pm 0.032$  (consistent with the *Planck* and RSD results shown in Fig. 4).

Figure 5 gives a summary of the results discussed in this Section. The two analyses that are most discrepant with the  $S_8$  value from *Planck* (CFHTLenS and K17) both have strongly negative intrinsic alignment solutions. The H17 results are in tension with *Planck* but become consistent with *Planck* with the addition of galaxy-galaxy and galaxy-mass data (vU17). The DES year 1 analyses plotted in Fig. 5 are both consistent with *Planck*. The intrinsic alignment solutions of vU17 and DES Collaboration et al. (2017) (i.e.  $A_{IA} \sim 1$ ) seem physically plausible given the mix of galaxy types expected in these surveys.

## 5 CONCLUSIONS

The main purpose of this paper has been to highlight and quantify internal inconsistencies in the KiDS cosmic shear analysis. Our main conclusion is that more effort is needed to resolve inconsistencies in the KiDS data. This includes understanding the origin of the B-modes, systematic differences between  $\xi_+$  and  $\xi_-$ , the parameter shifts seen by excluding photometric redshift bin 3, the large excess  $\chi^2$  and scatter at large angular scales. Until this is done, it seems premature to draw inferences on new physics from KiDS.

Comparison of *Planck* with other measures of the amplitude of the mass fluctuations, principally redshift space distortions from BOSS, reveals no evidence for any inconsistencies with the *Planck* base- $\Lambda$ CDM cosmology. We have also reviewed cosmic shear constraints on  $S_8$ , emphasising the degeneracy between intrinsic alignments and cosmology. As summarized in Fig. 5 the two analyses which yield the lowest values of  $S_8$  both have strongly negative values of  $A_{IA}$ . The DES 1 year analyses are consistent with the *Planck*  $\Lambda$ CDM value for  $S_8$  (Troxel et al. 2017; DES Collaboration et al. 2017) and give physically plausible values for  $A_{IA}$ . The H17 value of  $S_8$  from KiDS sits about  $2.3\sigma$  low compared to *Planck*, but is pulled upwards with the addition of galaxy-galaxy, galaxy-mass data (vU17). Overall, we conclude there is no strong evidence for any inconsistency between the *Planck*  $\Lambda$ CDM cosmology and measures of the amplitude of the fluctuation spectrum at low redshift.

## ACKNOWLEDGEMENTS

We thank Hiranya Peiris, Benjamin Joachimi, Fergus Simpson and the referee for helpful comments on the preprint version of this paper. We thank Frankie Nobis-Efstathiou for help with the early stages of this project. We also thank Anthony Challinor, Steven Gratton and members of the KiDS team for comments on aspects of this analysis. We also thank members of the *Planck* Parameters team. Pablo Lemos acknowledges support from an Isaac Newton Studentship at the University of Cambridge and from the Science and Technologies Facilities Council.

## REFERENCES

- Abbott T., et al., 2016, *Phys. Rev. D*, 94, 022001  
 Alam S., et al., 2016, preprint ([arXiv:1607.03155](https://arxiv.org/abs/1607.03155))  
 Alcock C., Paczynski B., 1979, *Nature*, 281, 358  
 Amendola L., et al., 2016, preprint ([arXiv:1606.00180](https://arxiv.org/abs/1606.00180))  
 Applegate D. E., et al., 2014, *MNRAS*, 439, 48  
 Blandford R. D., Saust A. B., Brainerd T. G., Villumsen J. V., 1991, *MNRAS*, 251, 600  
 Blazek J., MacCrann N., Troxel M. A., Fang X., 2017, preprint, ([arXiv:1708.09247](https://arxiv.org/abs/1708.09247))  
 Bridle S., King L., 2007, *New Journal of Physics*, 9, 444  
 DES Collaboration et al., 2017, preprint, ([arXiv:1708.01530](https://arxiv.org/abs/1708.01530))  
 Driver S. P., et al., 2011, *MNRAS*, 413, 971  
 Hasselfield M., et al., 2013, *J. Cosmology Astropart. Phys.*, 7, 008  
 Heymans C., et al., 2012, *MNRAS*, 427, 146  
 Heymans C., et al., 2013, *MNRAS*, 432, 2433  
 Hildebrandt H., et al., 2017, *MNRAS*, 465, 1454  
 Hinshaw G., et al., 2013, *ApJS*, 208, 19  
 Hirata C. M., Seljak U., 2004, *Phys. Rev. D*, 70, 063526  
 Huterer D., Shafer D. L., Scolnic D. M., Schmidt F., 2017, *J. Cosmology Astropart. Phys.*, 5, 015  
 Jee M. J., Tyson J. A., Hilbert S., Schneider M. D., Schmidt S., Wittman D., 2016, *ApJ*, 824, 77  
 Joachimi B., Mandelbaum R., Abdalla F. B., Bridle S. L., 2011, *A&A*, 527, A26  
 Joachimi B., et al., 2015, *Space Sci. Rev.*, 193, 1  
 Joudaki S., et al., 2016, preprint ([arXiv:1610.04606](https://arxiv.org/abs/1610.04606))  
 Joudaki S., et al., 2017, *MNRAS*, 465, 2033  
 Kaiser N., 1987, *MNRAS*, 227, 1  
 Kaiser N., 1992, *ApJ*, 388, 272  
 Kelly P. L., et al., 2014, *MNRAS*, 439, 28

- Kirk D., Rassat A., Host O., Bridle S., 2012, *MNRAS*, 424, 1647  
Köhlinger F., et al., 2017, preprint ([arXiv:1706.02892](#))  
Liske J., et al., 2015, *MNRAS*, 452, 2087  
Mantz A. B., et al., 2015, *MNRAS*, 446, 2205  
Miralda-Escude J., 1991, *ApJ*, 380, 1  
Planck Collaboration et al., 2014a, *A&A*, 571, A16  
Planck Collaboration et al., 2014b, *A&A*, 571, A20  
Planck Collaboration et al., 2016a, *A&A*, 594, A13  
Planck Collaboration et al., 2016b, *A&A*, 594, A15  
Planck Collaboration et al., 2016c, *A&A*, 594, A24  
Roza E., et al., 2010, *ApJ*, 708, 645  
Scolnic D., et al., 2015, *ApJ*, 815, 117  
Sievers J. L., et al., 2013, *J. Cosmology Astropart. Phys.*, 10, 060  
Springob C. M., et al., 2014, *MNRAS*, 445, 2677  
Story K. T., et al., 2013, *ApJ*, 779, 86  
Troxel M. A., Ishak M., 2015, *Phys. Rep.*, 558, 1  
Troxel M. A., et al., 2017, preprint, ([arXiv:1708.01538](#))  
Vikhlinin A., et al., 2009, *ApJ*, 692, 1060  
de Haan T., et al., 2016, *ApJ*, 832, 95  
van Uitert E., et al., 2017, preprint ([arXiv:1706.05004](#))  
von der Linden A., et al., 2014, *MNRAS*, 439, 2